RESEARCH PAPER

PCCP
www.rsc.org/pccp

Structures and infrared spectra of fluoride–hydrogen sulfide clusters from *ab initio* calculations: $F^-(H_2S)_n$, $n = 1–5$†

D. A. Wild* and T. Lenzer

MPI für biophysikalische Chemie, Abteilung Spektroskopie und Photochemische Kinetik (10100), Am Faßberg 11, D-37077 Göttingen, GermanyE-mail: dwild@gwdg.de. E-mail: tlenzer@gwdg.de; Fax: +49 551 201 1501; Tel: +49 551 201 2004

Received 1st August 2005, Accepted 6th September 2005
First published as an Advance Article on the web 22nd September 2005

Clusters formed between a fluoride anion and several hydrogen sulfide molecules have been investigated *via ab initio* calculations at the MP2 level of theory, using Dunning's augmented correlation consistent basis sets. Optimised geometries, vibrational frequencies, and enthalpy changes for the ligand association reactions are presented for clusters with up to five H_2S ligands interacting with a F^- anion. The minimum energy structure for the 1 : 1 F^--H_2S complex features proton transfer from the H_2S to the F^- anion, forming a planar C_s symmetry $FH\cdots SH^-$ structure. For the F^-–$(H_2S)_2$ cluster, the $FH\cdots SH^-$ core remains and is solvated by a perturbed H_2S ligand. For the larger F^-–$(H_2S)_{3–5}$ clusters, in addition to the $FH\cdots SH^-$–$(H_2S)_n$ cluster forms, other minima featuring a 'solvated F^-' anion are predicted. Calculated infrared spectra for the minima of each cluster size are presented to aid in assigning spectra from future experimental studies.

1. Introduction

Studies on the interactions between ions and solvent molecules have importance for more detailed descriptions of molecular interactions, and for describing ion solvation in bulk contexts.[1] To arrive at the structures and energetics for ionic clusters, *ab initio* and spectroscopic studies are invaluable. On the experimental front, photoelectron, infrared, and microwave spectroscopy of gas phase ion complexes and clusters have furnished qualitative, or in some cases quantitative, structural information and provided electron detachment energies.[2–23] *Ab initio* calculations of ion–solvent clusters have proved useful in rationalising experimental observations, and in guiding future experiments.[24–27] The combination of these two fields has proved extremely fruitful in recent years.

For obvious reasons, the solvation of ions by water has received a great deal of attention. In past studies, experiment[15,16,28–30] and theory [28,31–35] concur that the structures adopted by halide–water clusters depend on a balance of ion–solvent and solvent–solvent interactions. For example, in the fluoride–water clusters the anion–solvent binding forces dominate, resulting in the anion being situated in the interior of the structure.[28] For clusters involving the larger halides, the solvent–solvent attractive interactions play a more significant role in determining the cluster structure, the result being solvent–solvent bonds and structures where the anion binds to the surface of the solvent network. Experimental evidence of such a network is the absence of bands in the spectra due to free or non-bonded O–H oscillators,[29] and the introduction of ring modes similar to those seen for the neutral water trimer.[36,37] For a review on recent investigations into halide ion hydration, the reader is directed to ref. 38.

To the best of our knowledge no electronic structure calculations or experimental studies exist thus far for the fluoride–hydrogen sulfide clusters. This work constitutes an investigation of small clusters with up to five H_2S molecules interacting with a fluoride anion. One might assume that the structures of these species would not be too dissimilar to the analogous halide–water clusters. An interesting aspect of the current study, however, lies in the fact that the proton affinity of the F^- anion exceeds that of SH^- (371.3 kcal mol^{-1} *versus* 350.8 kcal mol^{-1}; refs. 39 and 40, respectively). It is therefore quite likely that, in the absence of a large reaction barrier, proton transfer will occur from H_2S to F^- thereby forming a $FH\cdots SH^-$ complex. This situation differs from the halide–water dimer complex which displays a $X^-\cdots HOH$ structure due to the larger proton affinity (PA) of OH^- compared with the halides (for example $PA(OH^-) = 390.3$ kcal mol^{-1} [41] compared with $PA(F^-) = 371.3$ kcal mol^{-1} [39])

Quite recently, a combined experimental and theoretical study was reported for the complex formed between O_2^- and H_2S.[42] In this paper, *ab initio* and density functional theory calculations confirmed a proton transferred minimum energy structure with $O_2H\cdots SH^-$ form. In this case, as with the fluoride–H_2S complex, the proton affinity of the interacting anion O_2^- exceeds that of SH^- (353.0 *versus* 350.8 kcal mol^{-1}; refs. 40 and 43). The calculated binding energy of this complex is reported to be $D_e = 14.4$ kcal mol^{-1}.

The question arises, will a $FH\cdots SH^-$ anion core persist when more H_2S ligands adhere, or will structures with a solvated F^- anion emerge, *i.e.* F^-–$(H_2S)_n$? If so, at what cluster size will this occur? In this study, we wish to determine the dominant solvation structures and we aim to provide infrared spectra that should prove helpful for assigning future experimental results should multiple isomers be present. In this respect, this paper is an extension of our recent work on the fluoride–ammonia anion clusters.[44] Our choice of computational methodology is guided by studies of the water–halide clusters. It has been shown that the MP2/aug-cc-pvxz (x = d,t) levels of theory are suitable choices for describing the halide–water systems.[28,31,34,35,45–47] The use of augmented basis sets is particularly important for adequately describing the diffuse electron clouds of anions.

† Electronic supplementary information (ESI) available: Results from calculations with aug-cc-pvdz and aug-cc-pvtz basis sets. See http://dx.doi.org/10.1039/b510923j

DOI: 10.1039/b510923j

2. Details of the calculations

The F^-–$(H_2S)_n$ clusters were investigated at the MP2 level of theory using Dunning's augmented correlation consistent polarized valence sets.[48–50] For the 1 : 1, 1 : 2, and 1 : 3 clusters, calculations were performed with basis sets of double and triple-ζ quality (aug-cc-pvxz where x = d,t). MP2/aug-cc-pvdz calculations were performed for the larger 1 : 4 and 1 : 5 clusters due to smaller computation times compared with using aug-cc-pvtz basis sets. Only the valence electrons were included in the MP2 calculations (frozen core approximation). Calculations were also performed for H_2S, HF, SH^-, and F^- to aid in predicting cluster intermolecular binding energies. Corrections to the binding energies for basis set superposition error (BSSE) were estimated using the method of Boys and Bernardi.[51] Harmonic vibrational frequencies were computed analytically. It should be remembered that these results are an overestimation of the actual values due to the neglect of anharmonicity. Natural bond order (NBO) analyses were performed on the clusters to determine the nature of the bonding between the cluster constituents.[52] Enthalpy changes for the ligand association reactions at 298 K were estimated using the method described in ref. 53. The geometry optimisations, energy and vibrational frequency calculations, and NBO analyses were performed with the GAUSSIAN-03 program suite.[54] Diagrams of the cluster structures were produced using the gOpenMol program.[55,56]

3. Results and discussion

A. F^-–H_2S

Results for the 1 : 1 'dimer' complex from MP2, CCSD, and CCSD(T) calculations using Dunning's augmented correlation consistent basis sets up to aug-cc-pvqz will be reported in a separate publication.[57] In this article we make anharmonic corrections to the harmonic *ab initio* frequencies using the vibrational self-consistent field method (vscf)[58,59] and other approximations. We found that for the geometrical parameters, increasing the basis set size past aug-cc-pvtz had only a small effect. Furthermore, differences using this set and the aug-cc-pvdz set are not drastically large. One finding of this study was anomalous results obtained from extended correlation consistent vscf theory (cc-vscf) for the complex at the MP2/aug-cc-pvtz level, where the predicted anharmonic F–H stretch value exceeded the harmonic value. This may be due to the cc-vscf procedure coupling modes that are essentially local in character in the cluster. The vscf results, omitting mode coupling, give the expected shift in the vibrational frequency to lower wavenumber adding weight to this argument. Here we provide the structures, energetics and harmonic vibrational frequencies of a minimum and two higher order stationary points.

I. Structure descriptions and cluster energies

C_s minimum. The minimum energy structure of the 1 : 1 complex displays C_s symmetry and has the $FH\cdots SH^-$ form shown in Fig. 1a. Optimised coordinates and vibrational frequencies are given in Table 1. The intermediate proton involved in the H-bond has transferred from H_2S to the F^- anion, which can readily be explained by the larger proton affinity of the F^- compared with SH^- (371.3 kcal mol^{-1} *versus* 350.8 kcal mol^{-1}; refs. 39 and 40 respectively). Attempts to locate a stationary point with an intact H_2S ligand solvating the fluoride anion, similar to that of the X^-–H_2O complexes,[31,46,60,61] failed as the structure converged to the C_s minimum shown in Fig. 1a. The calculated binding energy (D_0) of the complex is 22.7 kcal mol^{-1}, with respect to HF and SH^- products. The H-bond is weaker than the predicted association enthalpy of 26.5 kcal mol^{-1} for F^-–H_2O,[47] however stronger than the recently reported value of $D_e = 14.4$ kcal mol^{-1} for $O_2H\cdots SH^-$.[42]

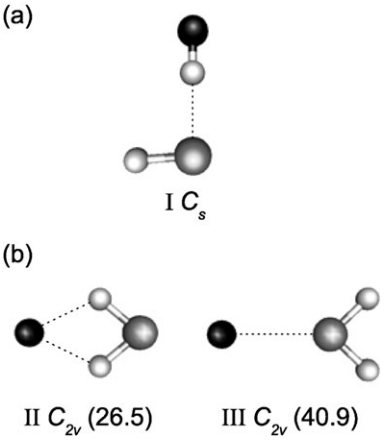

Fig. 1 Three stationary points found for the F^-–H_2S complex, (a) is the C_s symmetry minimum, (b) are two C_{2v} higher order stationary points. The energy differences between the stationary points and the C_s minimum are given in parentheses (kcal mol^{-1}). Optimised internal coordinates appear in Table 1.

Formation of the complex affects both HF and SH^- diatomics to different extents. The most obvious effect is elongation of the F–H bond ($\Delta r(F–H_b) = +0.064$ Å from Table 1), characteristic of H-bond formation.[65] This elongation is reflected in a redshift and marked intensity increase of the F–H stretch frequency (*vide infra*). The H–S^- bond length decreases slightly upon complex formation ($\Delta r = -0.002$ Å; Table 1).

Transition states. Two C_{2v} symmetry constrained stationary points were located. Both structures possess a single imaginary frequency corresponding to a concerted rocking and stretching motion of the H_2S towards the C_s minimum. The structures are labelled isomer II and III in Fig. 1b, and the imaginary frequencies are $575i$ and $261i$ cm^{-1}, respectively. Internal coordinates, energies and vibrational frequencies for these structures are provided in Table 1.

Isomer II is a doubly H-bonded structure (confirmed by NBO analysis, *vide infra*). After BSSE and zpe corrections are made, the energy difference between this transition state and the C_s minimum is 26.5 kcal mol^{-1}. Isomer III features the fluoride anion interacting with the sulfur of the H_2S. This stationary point lies some 40 kcal mol^{-1} to higher energy after BSSE and zpe corrections are made.

II. NBO analyses. NBO analyses were performed for the C_s minimum and isomer II to assess the nature of the cluster H-bonding. The results constitute molecular orbital occupancies (in m*e*) and second-order perturbation energies $E^{(2)}$ for electron density transfer donor → acceptor interactions (in kcal mol^{-1}). The signature of H-bonding is electron density transfer from lone pair orbitals of the H-bond acceptor to the anti-bonding orbital of the H-bond donor.

The NBO analysis for the C_s structure reveals significant electron density transfer from the lone pairs of the sulfur to the anti-bonding orbital of the F–H molecule (σ*). In total, the σ* orbital occupancy increases by 118 m*e*. The second-order perturbation energies $E^{(2)}$ reveal that the transfer from the lone pairs of the sulfur atom affords the greatest stabilisation. There is also a small amount of density transfer from core orbitals of the sulfur. The total stabilisation energy is 66.2 kcal mol^{-1} for transfer to the F–H antibonding orbital, of which 65.1 kcal mol^{-1} is accounted for by lone pair to σ* transfer. An NBO analysis was also performed on the F–H molecule in the complex geometry with the SH^- anion replaced with a point charge to determine the change in F–H orbital occupancies due

Table 1 Calculated data for the structures found for the 1 : 1 F^-–H_2S complex at MP2/aug-cc-pvtz. Provided are internal coordinates (r in Å and θ in degrees), harmonic vibrational frequencies (ω in cm^{-1}, intensities in km mol^{-1} in bold text, symmetries included), zpe (in kcal mol^{-1}), MP2 energies (E_{MP2} in hartrees), BSSE and zpe corrected energy differences ($\Delta E_{BSSE/Corr}$ in kcal mol^{-1}), and enthalpy change for the association reaction at 298 K ($\Delta H_{0\rightarrow1}{}^{298\ K}$ in kcal mol^{-1}). Also provided are data for bare H_2S, HF, SH^-, and F^-. Subscripts 'b' and 't' refer to H-bonded or terminal hydrogens, *e.g.* F–H_b

	F^-–H_2S		
	I	II	III
r(F–H_b)	0.986	2.028	2.827 r(F^-–S)
r($H_b\cdots$S)	1.968	1.354	
r(S–H_t)	1.340		1.348
θ(F–H_b–S)	179.2	114.5	136.22 θ(F–S–H_t)
θ(H–S–H)	94.3	80.1	87.6
ω_1	2833 **3014** a'	2663 a_1	2682 a_1
ω_2	2737 **69** a'	943 a_1	1200 a_1
ω_3	990 **25** a'	214 a_1	108 a_1
ω_4	304 **11** a'	570 b_1	321 b_1
ω_5	247 **29** a'	2594 b_2	2705 b_2
ω_6	884 **23** a''	575*i* b_2	261*i* b_2
zpe	11.4	10.0	10.0
E_{MP2}	−498.724857	−498.679693	−498.656213
$\Delta E_{BSSE/Corr}$	0.0	26.5	40.9
$\Delta H_{0\rightarrow1}{}^{298\ K}$	−22.7	—	—
	H_2S		
	aug-cc-pvdz	aug-cc-pvtz	
r(S–H)[a]	1.350 (14)	1.336 (0)	
θ(H–S–H)[a]	92.5 (4)	92.2 (1)	
ω_1 (a_1)	2755 **0***	2773 **0***	
ω_2 (a_1)	1193 **1**	1211 **1**	
ω_3 (b_2)	2780 **0***	2793 **1**	
zpe	9.6	9.7	
E_{MP2}	−398.853219	−398.908818	
	HF		
	aug-cc-pvdz	aug-cc-pvtz	
r(F–H)[a]	0.925(8)	0.922(5)	
ω_1 (σ_g)	4082 **116**	4123 **121**	
zpe	5.8	5.9	
E_{MP2}	−100.255805	−100.340891	
	HS^-		
	aug-cc-pvdz	aug-cc-pvtz	
r(S–H)[a]	1.356(16)	1.342(2)	
ω_1 (a_1)	2697 **82**	2717 **65**	
zpe	3.9	3.9	
E_{MP2}	−398.293255	−398.345321	
	F^-		
	aug-cc-pvdz	aug-cc-pvtz	
E_{MP2}	−99.745879	−99.745879	

[a] Numbers in parentheses are differences in the last significant figure between these calculations and experimental values taken from refs. 62–64.

to polarisation by the negative charge. No polarisation induced change in the σ* orbital occupancy was found.

The NBO analysis for isomer II confirms the double H-bond between H_2S and F^-, with the occupancy of each σ* orbital occupancy increasing by 13 m*e*. The stabilisation energy for each density transfer is 6.0 kcal mol^{-1}.

The σ* orbital occupancy predicted for the C_s minimum is an order of magnitude greater than that for the C_{2v} transition state. The difference can be rationalised by considering that the F–H–S intermolecular bond is much closer to linearity for the C_s complex compared with isomer II (179° *versus* 114°). This nearly linear H-bond leads to better overlap between the sulfur lone pair and F–H σ* orbitals and hence larger electron density transfer.

III. Predicted infrared spectrum. A stick spectrum of the calculated harmonic frequencies is presented in Fig. 2 (MP2/aug-cc-pvtz results). The vibrational modes are separated into two groups, the intermolecular stretching and bending vibrations below 1000 cm^{-1}, and the hydrogen stretching vibrations above 2700 cm^{-1}.

Looking to the hydrogen stretch region, the F–H stretch (labelled ω_{HF} in Fig. 2) is shifted some 1290 cm^{-1} to lower

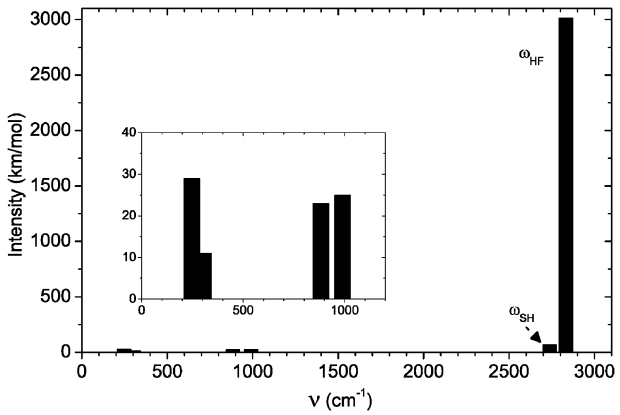

Fig. 2 Calculated infrared spectrum of the FH···SH$^-$ complex at the MP2/aug-cc-pvtz level. Frequencies are provided in Table 1.

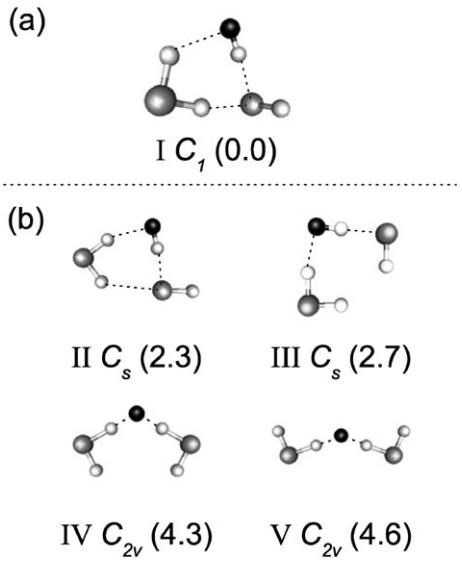

Fig. 3 Predicted structures for F$^-$–$(H_2S)_2$ clusters, with (a) the minimum with a FH···SH$^-$ core and (b) higher order stationary points.

frequency from the calculated harmonic frequency of bare HF (Table 1). The infrared intensity of this stretching vibration increases from 121 km mol^{-1} for bare HF to 3014 km mol^{-1} in the complex. Both the band shift and increased intensity are characteristic of strong H-bond formation.[65]

The SH stretch in the complex is blue shifted from that of bare SH$^-$ harmonic value by approximately 20 cm^{-1} (labelled ω_{SH} in Fig. 2) The blue shift reflects the decreased bond length ($\Delta r = -0.002$ Å; results in Table 1). There is little change in the infrared intensity of this vibration on complex formation.

It is hoped that the predicted infrared spectrum will aid future experimental studies, however it should be remembered that the reported frequencies are based on the harmonic approximation and hence should be scaled for anharmonicity. Furthermore, due to the large predicted binding energy of the complex (−22.7 kcal mol^{-1} or *ca.* 8100 cm^{-1}) vibrational predissociation spectroscopy is not applicable without resorting to the use of 'spy' atoms (recent examples of this technique can be found in refs. 38 and 66)

B. F$^-$–$(H_2S)_2$

The clustering of two H_2S ligands to a fluoride anion leads one to ask, does the FH···SH$^-$ core structure persist or, alternatively, is a cluster form with a fluoride anion core energetically favoured ('solvated F$^-$')? With this in mind we move to the discussion of the 1 : 2 'trimer' cluster, F$^-$–$(H_2S)_2$. Stationary points found from calculations at the MP2 level with the aug-cc-pvtz basis set are shown in Fig. 3. Selected data for the isomers are presented in Table 2, and a more extensive data set can be found in the electronic supplementary material.† While the MP2/aug-cc-pvtz level is considered a better choice due to the greater flexibility of the triple zeta basis set over the double zeta basis set, differences in the geometrical parameters are not so large. For comparison, the results from calculations with aug-cc-pvdz and aug-cc-pvtz basis sets can be found in the electronic supplementary material, the average deviation in bond lengths and angles is on the order of 0.01 Å and 1°, respectively.

I. Structure descriptions and NBO analyses

FH···SH$^-$–(H_2S) structures. Isomers I–III display the same structural motif as for the 1 : 1 cluster, *i.e.* a FH···SH$^-$ core. For isomer I the additional H_2S ligand forms two H-bonds, one with the sulfur of the SH$^-$ anion and a second with the fluoride of the HF moiety. For isomers II and III, the second H_2S forms an H-bond with the fluorine atom and points towards the SH$^-$, in one case H-bonding to the sulfur and in the other pointing towards the hydrogen of the SH$^-$. The nature of the cluster bonding is described below in terms of NBO analyses. Isomer I is the only minimum found for this cluster size. Isomers II and III are transition states, each with one imaginary frequency corresponding to rocking of the hydrogens of the SH$^-$ and H_2S, towards the minimum. The

Table 2 Selected data for the stationary points of the F$^-$–$(H_2S)_2$ clusters at the MP2/aug-cc-pvtz level, r in Å and θ in degrees. Also provided are zpe (in kcal mol^{-1}), MP2 energies (E_{MP2} in hartree), number of imaginary frequencies (img. freq.), BSSE and zpe corrected energy differences ($\Delta E_{BSSE/Corr}$ in kcal mol^{-1}), and for the minimum the ligand association enthalpy change at 298 K ($\Delta H_{1\rightarrow 2}{}^{298\ K}$ in kcal mol^{-1}). Subscripts 'b' and 't' refer to H-bonded or terminal hydrogens. Subscripts 'S' and 'F' refer to groups with H-bonds to sulfur and fluoride, respectively

	I	II	III	IV	V
r(F–H$_b$)	0.981	0.997	1.009	1.355	1.365
r(H$_b$···S)	1.980	1.921	1.884	1.477	1.471
r(S–H$_t$)	1.340	1.339	1.340	1.337	1.337
θ(F$^-$–H$_b$–S)	176.7	174.1	178.8	179.0	178.4
r(S–H$_S$)[a]	1.382	1.344			
r(S–H$_F$)[a]	1.338	1.341	1.350		
θ(H–S–H)[a]	90.4	90.5	91.0	93.2	93.3
zpe	22.5	22.1	21.9	19.1	19.1
img. freq.	0	1	1	2	3
E_{MP2}	−897.65303	−897.64851	−897.64751	−897.64129	−897.64074
$\Delta E_{BSSE/Corr}$	0.0	2.3	2.7	4.3	4.6
$\Delta H_{1\rightarrow 2}{}^{298\ K}$	−10.2				

[a] Data for intact solvating H_2S ligands.

magnitudes of the imaginary frequencies are 207*i* and 159*i* cm^{-1} for isomers I and II, respectively.

For the minimum (isomer I) the $FH\cdots SH^-$ core is altered only slightly from the 1 : 1 complex. The F–H bond length is contracted ($\Delta r(F–H_b) = -0.005$ Å; Table 2), while the intermolecular bond length is lengthened ($\Delta r(H_b\cdots S) = 0.012$ Å). Both of these changes indicate a reduction in the H-bond strength of the $FH\cdots SH^-$ core, confirmed by the NBO analysis. The F–H σ* orbital occupancy is 113 m*e*, compared with 118 m*e* for the dimer. The stabilisation energies are 60 and 66 kcal mol^{-1} for trimer and dimer, respectively. The NBO analysis also reveals that the interaction between the solvating H_2S and the $FH\cdots SH^-$ core is indeed H-bonding. There is electron density transfer from both the S and F lone pairs to the respective antibonding orbitals of the H_2S, where the former one is by far more important (74 compared with 2 m*e*).

The solvating H_2S molecule is distorted in the cluster compared with the bare molecule. The S–H bond length $r(S–H_S)$ associated with the $HSH\cdots SH^-$ hydrogen bond is elongated by 0.046 Å from that of bare H_2S (see Tables 1 and 2), while the S–H bond length associated with the $HSH\cdots FH$ H-bond is also elongated slightly by 0.002 Å. The H–S–H bond angle is decreased in the cluster by around 2°.

F^-–$(H_2S)_2$ structures. The two symmetry constrained F^-–$(H_2S)_2$ structures (labelled IV and V in Fig. 3b) are higher order stationary points possessing more than one imaginary frequency. Internal coordinates as well as energy separations between these isomers and the minimum are provided in Table 2. The two structures differ in the displacement of the H_2S ligands about the fluoride anion.

The largest effect of cluster formation on the H_2S ligands is observed in the H-bonded S–H bond length, which increases by $\Delta r(H_b–S) = 0.141$ and 0.135 Å for isomers IV and V, respectively. The terminal S–H bond lengths also increase slightly by $\Delta r(S–H_t) = 0.001$ Å. The H–S–H angles increase by approximately 1° for each structure.

Stationary points IV and V lie 4.3 and 4.6 kcal mol^{-1} above the C_1 minimum, and have 2 and 3 imaginary frequencies, respectively. We were unable to locate minima with the F^-–$(H_2S)_2$ form. When a H_2S–H_2S H-bonded structure, similar to that predicted for halide–$(H_2O)_2$ clusters[31,46,60,61] was used as starting geometry it converged to the C_1 minimum shown in Fig. 3a.

II. Predicted infrared spectrum of $FH\cdots SH^-$–(H_2S). Calculated harmonic vibrational frequencies for the five trimer structures are provided in the electronic supplementary material. Results for the C_1 minimum are shown as a stick spectrum in Fig. 4. Again it should be emphasised that these frequencies are based on the harmonic approximation. The intermolecular bending and stretching modes and the intramolecular H_2S bending modes appear to lower wavenumber (50–1200 cm^{-1}). To higher wavenumber, above 2000 cm^{-1}, lie the F–H and S–H stretching vibrations.

The most intense band at 2921 cm^{-1} (intensity = 2397 km mol^{-1}) corresponds to the F–H stretching motion (labelled ω_{HF} in Fig. 4). This band has blue shifted by approximately 90 cm^{-1} from the analogous band in the dimer complex, due to the weakening of the $FH\cdots SH^-$ H-bond from perturbation by the solvating H_2S. A second intense band at 2214 cm^{-1} (intensity = 1709 km mol^{-1}) arises from the solvating H_2S ligand and corresponds to motion of the hydrogen involved in the H-bond to the sulfur of the SH^- (labelled ω_{SHb} in Fig. 4). This band has shifted some 570 cm^{-1} to the red of the centroid of the symmetric and antisymmetric S–H stretches of bare H_2S (2783 cm^{-1} from the MP2/aug-cc-pvtz calculations in Table 1).

It is hoped that the predicted spectrum will be valuable for the interpretation of experimental studies. Unfortunately, as with the 1 : 1 complex, predissociation spectroscopy cannot be applied to the trimer cluster. The predicted binding energy of around 3570 cm^{-1} for the H_2S ligand to the $FH\cdots SH^-$ core exceeds the energy imparted to the molecule following absorption of a single infrared photon. It may be possible to probe the trimer cluster *via* argon predissociation or multiphoton spectroscopies.

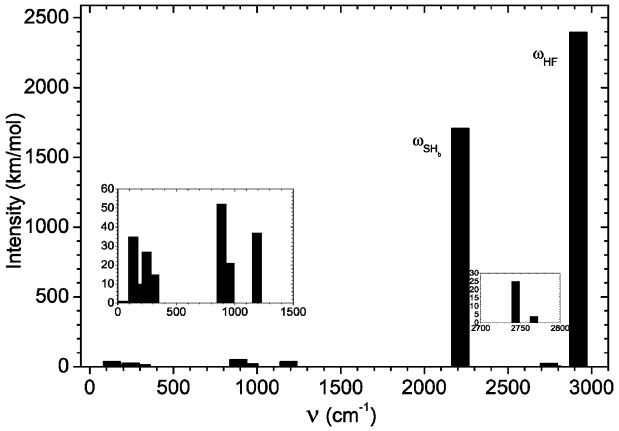

Fig. 4 Calculated infrared spectrum of the $FH\cdots SH^-$–(H_2S) minimum at the MP2/aug-cc-pvtz level. The insets are expanded plots of the low intensity bands. Frequencies, intensities, and band symmetries are provided in the electronic supplementary material.†

C. F^-–$(H_2S)_3$

The F^-–$(H_2S)_3$ 'tetramer' clusters were studied at the MP2 level of theory with both aug-cc-pvdz and aug-cc-pvtz basis sets. The difference in the structures and relative energies of the isomers for the two levels is small (refer to the data given in the electronic supplementary material†), leading us to believe that although the MP2/aug-cc-pvtz is more sophisticated, the lower aug-cc-pvdz basis set should still give a satisfactory representation of the bonding in this case.

I. Structure descriptions and NBO analyses. Eight stationary points, shown in Fig. 5, were located for the F^-–$(H_2S)_3$ cluster at the MP2/aug-cc-pvtz level of theory. Calculated data and harmonic vibrational frequencies at the MP2 level with aug-cc-pvdz and aug-cc-pvtz basis sets are provided in the electronic supplementary material.† Selected data for the minima are provided in Table 3.

Five minima were located, one with C_s symmetry (isomer I), three with C_1 symmetry (isomers II–IV) and one with C_3 symmetry (isomer V). The C_s and three C_1 symmetry minima feature the $FH\cdots SH^-$ core predicted for the dimer complex solvated by two perturbed H_2S ligands. In contrast, the C_3 isomer features a pyramid of H_2S ligands bound to a F^- core anion. This is the first occurrence of a minimum with a 'solvated F^-' cluster structure, as for the dimer and trimer we found only higher order stationary points with this structural motif.

Three higher order stationary points were also found, and are shown in Fig. 5b (isomers VI and VII with C_s symmetry and isomer VIII with C_{3h} symmetry). Similar to the isomer I, isomer VI features a $FH\cdots SH^-$ core solvated by perturbed H_2S ligands. The C_s symmetry structure (labelled isomer VII) features a central F^- anion surrounded by non-equivalent intact H_2S ligands. Finally, the C_{3h} symmetry isomer VIII features three equivalent H_2S ligands surrounding the F^- core. The following discussion will concentrate solely on the minima.

$FH\cdots SH^-$–$(H_2S)_2$ minima. For isomer I, the $FH\cdots SH^-$ core is only slightly affected by the presence of the additional H_2S ligands. Compared with the trimer cluster the F–H bond length decreases slightly ($\Delta r(F–H_b) = -0.001$ Å), and the

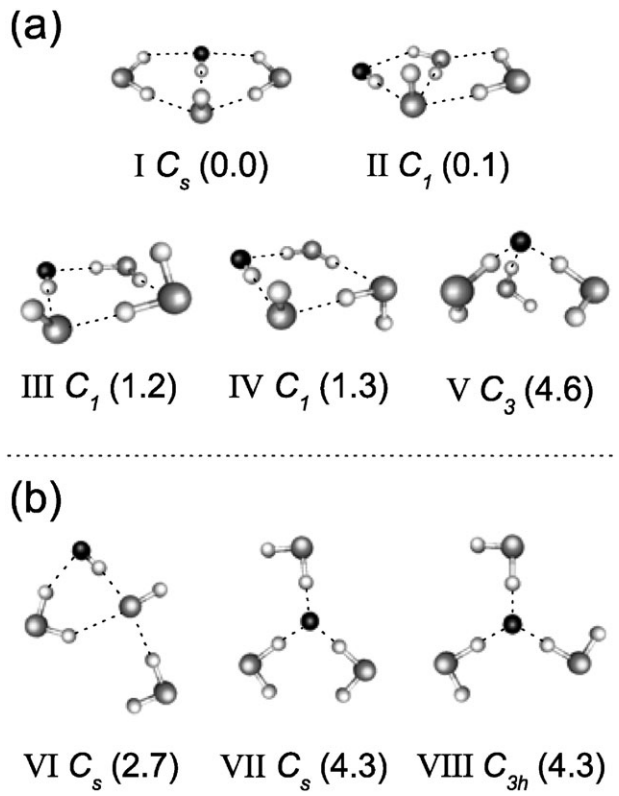

Fig. 5 Eight predicted stationary points for the 1 : 3 F^-–$(H_2S)_3$ clusters at the MP2/aug-cc-pvtz level of theory. (a) Corresponds to the minima, while (b) are higher order stationary points. The C_s symmetry isomer I is the lowest energy structure. Selected internal coordinates for the minima are in Table 3.

intermolecular bond length, $r(H_b\cdots S)$, is slightly shorter by 0.002 Å. The effect of cluster formation on the two 'intact' H_2S ligands is seen in the elongation of the S–H bonds, with Δr(S–H) = +0.002 and +0.032 Å for the hydrogens pointing towards the fluorine and sulfur, respectively (refer to supplementary material for full data set†). The increased bond lengths are consistent with H-bonding, and are confirmed by an NBO analysis for this structure. The σ* orbital occupancies for the two S–H bonds are 2 and 52 m*e*, respectively, while the stabilisation energies for the electron density transfer are 0.5 and 20.9 kcal mol^{-1}, respectively. One can see that the $HS^-\cdots$HSH H-bond is much stronger than the corresponding $HF\cdots$HSH interaction.

The $FH\cdots SH^-$ core is perturbed more in isomer II than in isomer I. Comparing the core with the trimer cluster, the $F–H_b$ bond length reduces by $\Delta r(F–H_b) = -0.008$ Å, and the H-bond length increases by $\Delta r(S\cdots H_b) = +0.029$ Å. The NBO analysis for this structure reveals that the interaction is weaker than for the trimer cluster, with the orbital occupancy and stabilisation energy being 97 m*e* and 53.8 kcal mol^{-1} compared with 113 m*e* and 60 kcal mol^{-1}. The intact H_2S ligands are bound to the core *via* H-bonds. For the H_2S ligand bound to the HF and SH^- moieties, the orbital occupancies and stabilisation energies are 3 and 61 m*e* and 0.3 and 25.8 kcal mol^{-1}, respectively. The other H_2S ligand is H-bonded to the SH^- moiety and the other intact H_2S. The corresponding orbital occupancies and stabilisation energies are 61 and 3 m*e* and 25.8 and 0.5 kcal mol^{-1}.

Interestingly, for isomers III and IV the F–H bond is lengthened, and the $S\cdots H_b$ H-bond is shortened, when compared with the dimer and trimer clusters. For example, for isomer III the F–H bond length is $r(F–H_b) = 0.988$ Å, while for the trimer and dimer the values are $r(F–H_b) = 0.981$ and 0.986 Å, respectively. The NBO analysis reveals that the orbital occupancy of the σ* antibonding orbital of the F–H fragment is 128 m*e*, while the corresponding values for the trimer and dimer are 113 and 118 m*e*, respectively. The density is transferred predominantly from the sulfur of the SH^- moiety (core, lone pair, and bonding orbital transfer). The $H_b\cdots SH^-$ hydrogen bond length is shorter in the tetramer compared with the trimer and dimer ($r(H_b–S) = 1.940$, 1.980, 1.968 Å for tetramer, trimer, and dimer, respectively). Both of these results indicate that the H-bond of the $FH\cdots SH^-$ core is stronger than in the dimer or trimer clusters. The strengthened H-bond may be attributed to the effect of the H_2S ligands drawing the HF and SH^- moieties closer together, as the ring is formed, leading to greater electron density transfer from the HS^- to HF.

Adding weight to this argument is the fact that the H-bonds of the H_2S ligands forming the ring are stronger than for the minimum of the trimer clusters. Firstly, for the doubly bonded H_2S, the orbital occupancies are 10 and 11 m*e*, respectively, for the S–H bonds pointing towards F and H_2S. For the other H_2S forming the H-bond with the sulfur of SH^-, the orbital occupancy is 102 m*e*. For comparison, in the trimer structure the orbital occupancies of the two S–H groups are 74 and 2 m*e* for H-bonds to SH^- and F–H respectively. The increased strength results from the H-bonds being closer to linearity in the tetramer compared with the trimer as can be clearly seen in Figs. 3 and 5.

F^-–$(H_2S)_3$ minimum. For the C_3 symmetry F^-–$(H_2S)_3$ cluster (isomer V), distortions of the hydrogen sulfide ligands are evident from association with the fluoride anion, however the ligands are generally less perturbed than in the analogous F^-–$(H_2S)_2$ trimer cluster. The H-bonded S–H bond lengths are elongated relative to the calculated structure of bare H_2S, with $r(S–H_b) = 1.571$ Å compared with $r(S–H) = 1.336$ Å (aug-cc-pvtz results for H_2S, refer to Table 1). The intramolecular H_2S angle is less than the one in the bare molecule, $\theta(H–S–H) = 91.5°$ and $\theta(H–S–H) = 92.2°$, respectively. The $F^-\cdots$HSH

Table 3 Selected data for the minima of the F^-–$(H_2S)_3$ clusters at the MP2/aug-cc-pvtz level of theory, *r* in Å and θ in degrees. Also provided are zpe in kcal mol^{-1}, MP2 energies (E_{MP2} in hartree), energy differences corrected for BSSE and zpe ($\Delta E_{BSSE/Corr}$ in kcal mol^{-1}), and incremental ligand association enthalpy change for the C_s symmetry lowest energy structure ($\Delta H_{2\rightarrow3}^{298\ K}$ in kcal mol^{-1}). Subscripts 'b' and 't' refer to H-bonded or terminal hydrogens, *e.g.* $F–H_b$

	I	II	III	IV	V
$r(F–H_b)$	0.980	0.973	0.988	0.986	1.571
$r(H_b\cdots S)$	1.978	2.009	1.940	1.946	1.400
$r(S–H_t)$	1.340	1.340	1.339	1.339	1.338
$\theta(F^-–H_b\cdots S)$	179.8	177.1	176.5	176.7	174.0
$\theta(H_b–S–H)$	92.8	91.7	95.8	95.8	91.5
zpe	33.4	33.4	33.2	33.1	31.9
E_{MP2}	−1296.57849	−1296.57841	−1296.57660	−1296.57616	−1296.56906
$\Delta E_{BSSE/Corr}$	0.0	0.1	1.2	1.3	4.6
$\Delta H_{2\rightarrow3}^{298\ K}$	−8.6				

H-bonds are further from linearity compared with the F^-–$(H_2S)_2$ clusters.

The NBO analysis for this isomer revealed that there are very weak $H_2S\cdots HSH$ H-bonds formed in the cluster. The σ* orbital occupancies of the H-bonded S–H groups are increased by approximately 2 m*e*, while the stabilisation energy is around 0.18 kcal mol^{-1}. These bonds are quite weak when compared with the $F^-\cdots HSH$ H-bonds, where the S–H σ* orbital occupancies are increased by 62 m*e* and the stabilisation energies are on the order of 36 kcal mol^{-1}.

II. Cluster energies. After BSSE and zero point energy difference corrections are made, isomer I lies only 0.1 kcal mol^{-1} below isomer II, and 1.2 and 1.3 kcal mol^{-1} below isomers III and IV, respectively. The C_3 symmetry isomer V lies 4.6 kcal mol^{-1} above isomer I. These results indicate that the $FH\cdots SH^-$–$(H_2S)_2$ cluster form should be the dominant arrangement formed in experimental studies, however with such a small energy difference between isomers I and II one cannot state conclusively which is the global minimum. The energy separations between isomer I and the higher order stationary points are greater than 2.7 kcal mol^{-1}.

III. Predicted infrared spectra. Calculated harmonic frequencies for all stationary points are provided in the supplementary material,† while stick spectra for the five minima are shown in Fig. 6. As for the trimer and dimer clusters, the vibrations can be separated into the low frequency intermolecular motions and H_2S intramolecular bends (below 1500 cm^{-1}), and the hydrogen stretching vibrations (above 1500 cm^{-1}). As the intermolecular and H_2S bending vibrations are quite weak (see the electronic supplementary information),† the following discussion will concentrate on the hydrogen stretching modes. These modes are most affected by complex formation, specifically by cluster hydrogen bonding. Looking to the stick spectra in Fig. 6 one can see that, apart from isomers III and IV, differences exist between the spectra that should prove useful in discriminating which isomers are observed experimentally.

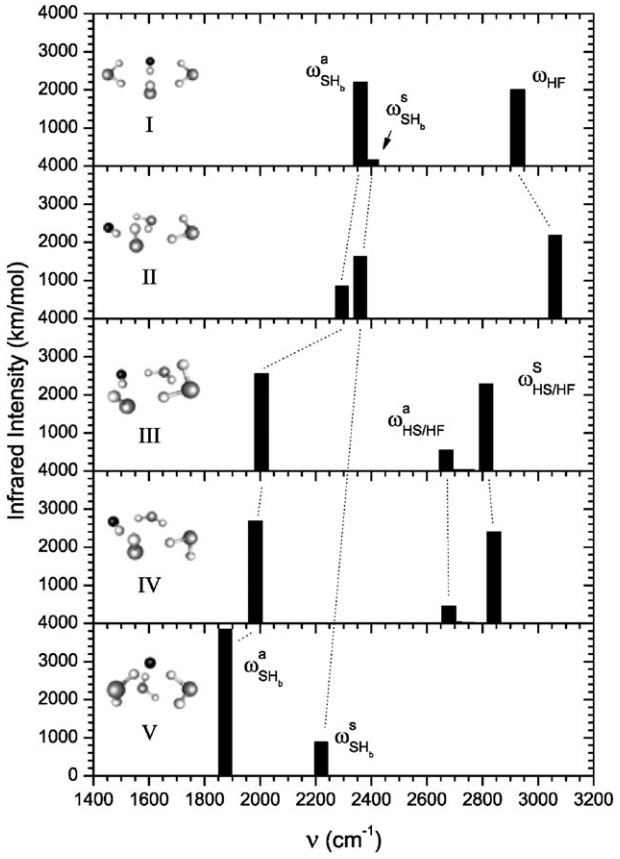

Fig. 6 Calculated infrared spectra of 1 : 3 F^-–$(H_2S)_3$ clusters at the MP2/aug-cc-pvtz level. Vibrations with similar forms are linked by dotted lines. See text for the band notation. Predicted frequencies, infrared intensities, and band symmetries are provided in the electronic supplementary material.†

Isomers I and II. For both isomers I and II, the band to highest wavenumber corresponds to the F–H stretch, labelled ω_{HF} in Fig. 6. The isomer II band lies higher than the corresponding isomer I reflecting the weaker $FH\cdots SH^-$ H-bond as highlighted in the discussion of the structures and NBO analyses. Two bands appear around 2300 cm^{-1}, and correspond to the concerted antisymmetric and symmetric stretches of the S–H groups H-bonded to $S(H)^-$, labelled $\omega^{a/s}_{HS_b}$. The other SH stretches have predicted infrared intensities below 12 km mol^{-1}.

Isomers III and IV. For both isomers III and IV, two bands appear above 2600 cm^{-1}. The band to highest wavenumber is predominantly the F–H stretch, however also involves some motion of the H-bonded hydrogen of the intact H_2S (forming the bond with the fluorine). This motion is a symmetric type stretch. The weaker band is the antisymmetric counterpart of this stretching motion, and in this case involves predominantly motion of the SH, with some motion of the HF. These bands are labelled as $\omega^s_{HS/HF}$ and $\omega^a_{HS/HF}$, respectively, in Fig. 6.

The most intense bands in both spectra are the stretching motion of the S–H group of the intact H_2S forming the H-bond to the SH^-.

Isomer V. Finally, looking to the C_3 symmetry isomer V, the highest wavenumber band corresponds to the concerted symmetric stretch of the three H-bonded hydrogens, labelled $\omega^s_{SH_b}$. The intense band is the doubly degenerate antisymmetric stretch, labelled $\omega^a_{SH_b}$. The symmetric and antisymmetric stretches of the terminal hydrogens have predicted infrared intensities below 1 km mol^{-1}.

C. F^-–$(H_2S)_4$

Calculations for the 1 : 4 'pentamer' cluster were performed using the aug-cc-pvdz basis set, as using the larger aug-cc-pvtz set would require more computation time than is currently feasible. We believe, following our investigations of the smaller clusters, that the differences between aug-cc-pvdz and -pvtz sets should not be large.

The key issue of this cluster size is whether the 'solvated F^-' cluster structures dominate. Many starting geometries were trialled to sample the largest part of the potential energy surface possible. In total, we found nine minima and two higher order stationary points. The nine minima are shown in Fig. 7, while a complete data set for all the structures (including the higher order stationary points) can be found in the electronic supplementary material.† Selected data for the minima are given in Table 4. Of the nine minima, five have a $FH\cdots SH^-$–$(H_2S)_3$ form, while the remaining four displayed the 'solvated F^-' structure (F^-–$(H_2S)_4$). The two higher order stationary points that we located have C_{4h} and C_s symmetry (refer to the electronic supplementary material).† Both correspond to 'solvated F^-' structures.

I. Structure descriptions and NBO analyses

$FH\cdots SH^-$–$(H_2S)_3$ structures. The isomers shown in Fig. 7a build on the C_s symmetry minimum of the tetramer cluster (isomer I), while those in Fig. 7b follow from the tetramer isomers II–IV.

The lowest energy structures correspond to those built on the C_s tetramer lowest energy structure (Isomers I–III in Fig. 7a). These isomers differ in the placement of the H_2S ligand

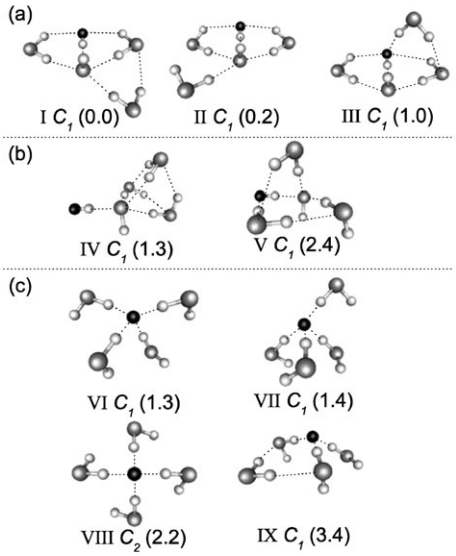

Fig. 7 Predicted minima for the F^-–$(H_2S)_4$ clusters at the MP2/aug-cc-pvdz level of theory. Sections (a) and (b) correspond to minima with a FH···SH^- core, while (c) are structures with a F^- core. Isomer I is the lowest energy structure, numbers in parentheses are BSSE and zpe corrected energy separations from the lowest energy structure. Selected internal coordinates appear in Table 4.

around the tetramer structure (Fig. 5a). NBO analyses confirmed that in each case the satellite H_2S ligand is attached *via* H-bonding. For isomer I, the H_2S ligand is bound to the SH^- moiety and one of the other H_2S ligands. The σ* orbital occupancies and stabilisation energies are 47 m*e* and 3.2 kcal mol^{-1} for the H-bond to SH^- and 4 m*e* and 1.0 kcal mol^{-1} for the H-bond to H_2S. For isomer II, the satellite H_2S is also bound to the SH^-, and weakly to another H_2S. In this case, the NBO predicts orbital occupancies and stabilisation energies of 48 and 3 m*e* and 6.2 and 0.7 kcal mol^{-1}, respectively. Finally, for isomer III the H_2S binds to both the HF and to one of the H_2S ligands in contact with the FH···SH^- core. The orbital occupancies and stabilisation energies are 12 m*e* and 6.8 kcal mol^{-1} for the HSH···FH H-bond, and 11 m*e* and 4 kcal mol^{-1} for the HSH···SH H-bond.

Looking now to isomer IV, the H_2S ligands interact exclusively with the SH^- moiety, while in the V isomer, one of the H_2S ligands interacts with the HF moiety. NBO analyses performed for the two structures reveal that the interactions between the cluster constituents are indeed H-bonds. The analysis predicts significant electron density transfer from the lone pair orbitals of the H-bond acceptor to the antibonding orbitals of the H-bond donor. H_2S···HSH and HSH···SH^- hydrogen bonds are formed in both of these isomers. For the V isomer, there is also evidence for a HF···HSH hydrogen bond. The cluster H-bonding is reflected in lengthened S–H bonds compared to bare H_2S (refer to electronic supplementary material, aug-cc-pvdz results).†

F^-–$(H_2S)_4$ structures. The four remaining isomers shown in Fig. 7c have the 'solvated F^-' form with intact H_2S ligands arranged around a F^- anion core. Three of the isomers display C_1 symmetry (VI, VII, and IX), while the fourth has C_2 symmetry with two sets of equivalent H_2S ligands (isomer VIII).

The main structural change of H_2S ligands is an increase in the H-bonded S–H bond length. The calculated bare H_2S bond length of r(SH) = 1.350 Å (MP2/aug-cc-pvdz calculations, Table 1) increases to 1.387–1.430 Å. The terminal SH bonds do not increase markedly.

The NBO analyses for these isomers reveal H-bonding between the H_2S constituents. The strongest case is seen in isomer IX, for the H_2S bound to two other H_2S ligands. The stabilisation energy for the lone pair → σ* electron density transfer is around 8–9 kcal mol^{-1} for each H-bond. This is expected as these H-bonds hold the H_2S in place. The stabilisation energies for the other isomers are much smaller (on average 0.5 kcal mol^{-1}) indicating that the H_2S–HSH H-bonds, while present, are quite weak. For comparison, in isomer VI the F^-···HSH bonds have stabilisation energies on the order of 32–42 kcal mol^{-1} and σ* orbital occupancies of around 43–56 m*e*.

II. Cluster energies. After BSSE and zero point energy difference corrections, we find that isomer I is the lowest energy structure. The energy difference between isomers I and II is however only 0.2 kcal mol^{-1}. With such a small energy difference it is impossible to state conclusively which isomer is actually the global minimum as significant error is introduced by using harmonic frequencies to calculate zero point energies. What we can say, however, is that both isomers I and II having the FH···SH^-–$(H_2S)_3$ form lie more than 1 kcal mol^{-1} lower than the F^-–$(H_2S)_4$ cluster forms, and hence may be favoured in experimental cluster studies. Of the F^-–$(H_2S)_4$ cluster forms, isomers VI and VII are the lowest energy forms, while the remaining two isomers VIII and IX lie to higher energy by around 1–2 kcal mol^{-1}.

Table 4 Selected data for minima of F^-–$(H_2S)_4$ at the MP2/aug-cc-pvdz level of theory, r in Å and θ in degrees. For the FH···SH^-–$(H_2S)_3$ cluster forms (isomers I–V) the data correspond to the FH···SH^- core, while for the F^-–$(H_2S)_4$ clusters a range of values is provided for the solvating H_2S ligands (isomers VI–IX). Also provided are zero point energies (zpe in kcal mol^{-1}), MP2 energies (E_{MP2} in hartree), energy differences between isomers corrected for BSSE and zpe ($\Delta E_{BSSE/Corr}$ in kcal mol^{-1}), and incremental ligand association enthalpy change for the C_1 symmetry lowest energy structure ($\Delta H_{3\rightarrow4}{}^{298\ K}$ in kcal mol^{-1}). Subscripts 'b' and 't' refer to H-bonded or terminal hydrogens, *e.g.* F–H_b

	I	II	III	IV	V	VI	VII	VIII[b]	IX
r(F–H_b)	0.976	0.976	0.997	0.967	0.985	1.630–1.693	1.660–1.681	1.684 *t*/*b* 1.680 *l*/*r*	1.501–1.666
r(H_b···S)	2.013	2.018	1.932	2.061	1.973	1.387–1–399	1.390–1.392	1.389/1.390	1.392–1.430
r(S–H_t)	1.353	1.354	1.354	1.353	1.354	1.350–1.351	1.350–1.351	1.351	1.350–1.351
θ(F^-–H_b–S)	178.8	179.1	177.5	179.6	174.0	172.3–175.7	171.6–173.5	176.6/173.1	174.1–179.3
θ(H–S–H)	96.4	91.8	92.1	96.1	88.5	91.6–92.4	91.4–92–0	91.8/91.9	91.9–93.0
zpe	44.0	44.0	43.8	44.3	44.2	43.1	43.3	43.3	42.7
E_{MP2}	−1695.198223	−1695.197936	−1695.196611	−1695.197605	−1695.195754	−1695.194551	−1695.195068	−1695.193520	−1695.191589
$\Delta E_{BSSE/Corr}$	0.0	0.2	1.0	1.3	2.4	1.3	1.4	2.2	3.4
$\Delta H_{3\rightarrow4}{}^{298\ K}$	−6.7[a]								

[a] This value is calculated using MP2/aug-cc-pvdz results for the tetramer minimum given in the electronic supplementary material. [b] *t*/*b* and *l*/*r* refer to the top/bottom and left/right H_2S ligands for this isomer (see Fig. 7(c)). Where two values are given, the first corresponds to *t*/*b* and the second to *l*/*r*.

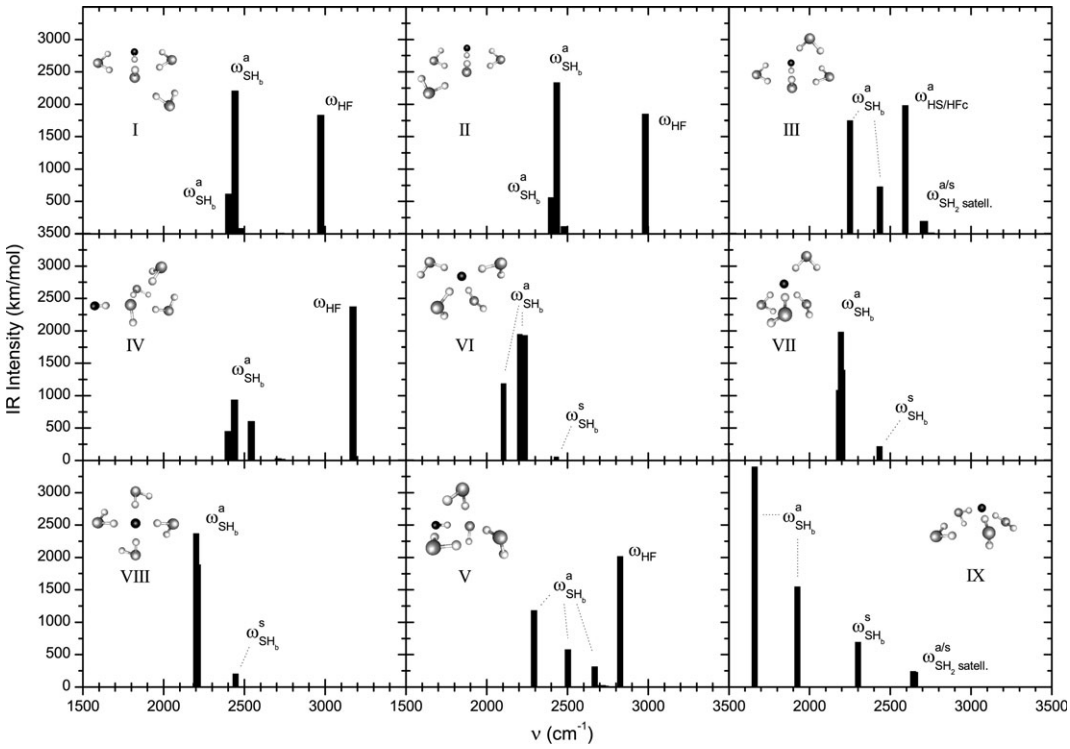

Fig. 8 Predicted infrared spectra for the F^-–$(H_2)_4$ 1 : 4 clusters over the 1500–3500 cm^{-1} range from MP2/aug-cc-pvdz calculations. The spectra are ordered from top left to bottom right in order of cluster stability. The full set of vibrational frequencies can be found in the electronic supplementary material.† See text for the definition of the band notation.

III. Predicted infrared spectra. The predicted vibrational frequencies for each isomer, along with associated symmetries and infrared intensities, can be found in the electronic supplementary material.† Stick spectra for the nine minima are shown in Fig. 8. The most intense bands correspond to the hydrogen stretching vibrations, and lie above 1600 cm^{-1}. The intramolecular H_2S bending and intramolecular stretching and bending modes lie below 1600 cm^{-1} (not shown in Fig. 8). The bands are labelled using the same notation used previously, with ω_{HF} the F–H stretch, $\omega^{a/s}_{HS/HF}$ an antisymmetric or symmetric concerted S-H/F-H stretching mode, and $\omega^{a/s}_{HS_b}$ an antisymmetric or symmetric stretching mode of H-bonded S–H groups. For isomers III and IX, the band labelled $\omega^{a/s}_{SH_2satell.}$ corresponds to the antisymmetric and symmetric S–H stretches of the satellite H_2S fragment.

In general, the bands with largest predicted intensities correspond to stretching modes of the H-bonded S–H groups, and the F–H stretch. Bands corresponding to 'free' S–H stretching modes have very low predicted intensities, and would be difficult to observe experimentally. Aside from isomers I and II and isomers VII and VIII, there are marked differences between the spectra which should aid in assigning experimental spectra when produced. Again, it should be emphasised that the predicted spectra shown here are based on the harmonic approximation.

D. F^-–$(H_2S)_5$

As for the 1 : 4 clusters, calculations for 1 : 5 'hexamer' cluster F^-–$(H_2S)_5$ were performed with the aug-cc-pvdz basis set, as using the larger aug-cc-pvtz set would require more computation time than is practical. We believe that this level should be adequate for obtaining good estimates for the structures and infrared spectra. Eight minima were found for this cluster size, and are shown in Fig. 9, with selected data given in Table 5. The structures are separated into three subsets. Set (a) features 'solvated F^-' structural motifs, isomers in set (b) are built on the C_s isomer I of the tetramer clusters, while those in set (c) are based on the C_1 symmetry structures of the tetramer (isomers II–IV). Sets (b) and (c) have the form of a $FH\cdots SH^-$ anion core solvated by H_2S ligands.

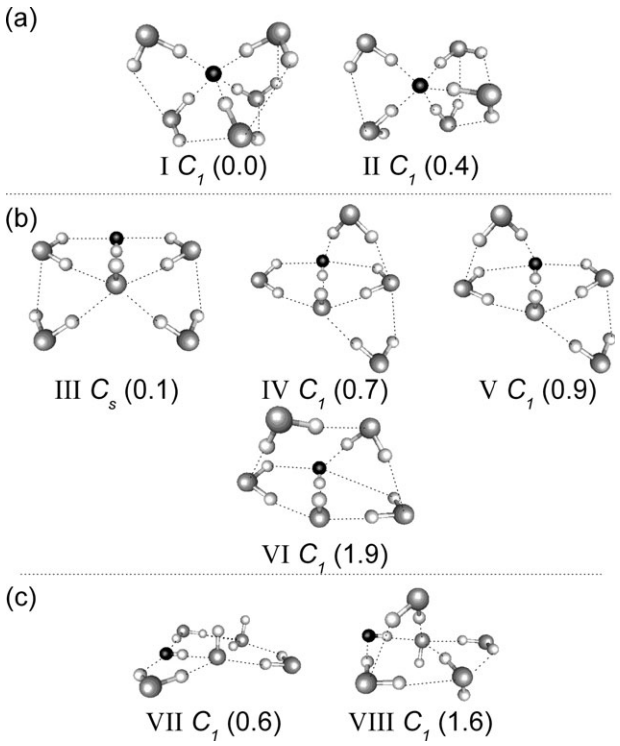

Fig. 9 Predicted minima for the F^-–$(H_2S)_5$ clusters at the MP2/aug-cc-pvdz level of theory. Section (a) corresponds to minima with a F^- core, while (b) and (c) are structures with a $FH\cdots SH^-$ core. Isomer I is the lowest energy structure, numbers in parentheses are BSSE and zpe corrected energy separations from this isomer. Selected internal coordinates appear in Table 4. Isomer III is of C_s symmetry, the rest are of C_1 symmetry.

Table 5 Selected data for minima of the F^-–$(H_2S)_5$ clusters at the MP2/aug-cc-pvdz level of theory, r in Å and θ in degrees. For the $FH\cdots SH^-$–$(H_2S)_4$ cluster forms the data correspond to the $FH\cdots SH^-$ core, while for the F^-–$(H_2S)_5$ cluster forms a range of values is given for the solvated ligands. Also provided are zpe in kcal mol^{-1}, MP2 energies (E_{MP2} in hartrees), energy differences between isomers corrected for BSSE and zpe ($\Delta E_{BSSE/Corr}$ in kcal mol^{-1}), and incremental association enthalpy change for the C_1 symmetry lowest energy structure ($\Delta H_{4\rightarrow5}{}^{298\ K}$ in kcal mol^{-1}). Subscripts 'b' and 't' refer to H-bonded or terminal hydrogens, *e.g.* F–H_b

	I	II	III	IV	V	VI	VII	VIII
r(F–H_b)	1.732–1.790	1.722–1.785	0.971	0.988	0.988	0.997	0.983	0.977
r($H_b\cdots$S)	1.376–1.383	1.376–1.383	2.031	1.955	1.954	1.927	1.979	2.000
r(S–H_t)	1.351–1.352	1.351–1.351	1.353	1.354	1.354	1.354	1.353	1.354
θ(F^-–H_b–S)	169.6–172.3	169.6–174.7	178.1	177.7	177.6	177.5	178.2	174.0
θ(H–S–H)	91.2–91.6	91.0–92.1	98.8	94.0	94.3	93.9	95.1	91.1
zpe	54.4	54.5	55.0	54.8	54.9	54.8	54.8	55.1
E_{MP2}	−2094.065047	−2094.064488	−2094.065521	−2094.064547	−2094.064435	−2094.063572	−2094.064185	−2094.064374
$\Delta E_{BSSE/Corr}$	0.0	0.4	0.1	0.7	0.9	1.9	0.6	1.6
$\Delta H_{4\rightarrow5}{}^{298\ K}$	−7.5[a]							

[a] Calculated with respect to the most stable 'solvated F^-' pentamer structure at MP2/aug-cc-pvdz.

I. Structure descriptions and NBO analyses

F^-–$(H_2S)_5$ structures. The two isomers in Fig. 9a are each of C_1 symmetry (labelled I and II). These isomers differ subtly in the arrangement of the H_2S ligands around the F^- anion core. Each isomer displays multiple $H_2S\cdots$HSH H-bonds, predicted from the NBO analysis and shown as dotted lines between the ligands in Fig. 9a. The average stabilisation energy for the $H_2S\cdots$HSH H-bonds is only around 0.7 kcal mol^{-1}, while the σ* orbital occupancy is around 3 m*e* for each H-bond. For comparison, the $F^-\cdots$HSH H-bonds have stabilisation energies of 20–26 kcal mol^{-1} and the σ* orbital occupancies are 34–38 m*e*. The larger H-bond strength for the $F^-\cdots$HSH *versus* $HSH\cdots SH_2$ bonds is reflected in the corresponding S–H bond lengths, where the range of values is r(H_b–S) = 1.376–1.383 Å and r(S–H_t) = 1.351–1.352 Å, respectively (Table 4). For comparison, the calculated S–H bond length of free H_2S at MP2/aug-cc-pvdz is 1.350 Å (see Table 1).

The H_2S ligands are less perturbed for this cluster size compared to the those in the F^-–$(H_2S)_4$ clusters. The H-bonded S–H bond lengths are smaller by around 0.01–0.1 Å, which can be explained by the weakening of the intermolecular $F^-\cdots$HSH bonds on addition of a further H_2S ligand. For example, the stabilisation energies and σ* orbital occupancies for isomer VI of the F^-–$(H_2S)_4$ clusters are in the range 32–42 kcal mol^{-1} and 43–56 m*e*, respectively.

$FH\cdots SH^-$–$(H_2S)_4$ structures. The four isomers shown in Fig. 9b build on the C_s isomer of the tetramer and differ in the arrangement of the two additional H_2S ligands. Isomer III features both H_2S ligands below the tetramer C_s unit and is the lowest energy isomer for this cluster set. Both ligands form H-bonds to the SH^- moiety, and also to one of the H_2S ligands in contact with the $FH\cdots SH^-$ core. The stabilisation energies are 15.8 and 1.1 kcal mol^{-1} for the $HSH\cdots SH^-$ and $HSH\cdots SH_2$ interactions, respectively. As a consequence of the stronger H-bonds, the S–H bond lengths associated with the $HSH\cdots SH^-$ interaction are longer by 0.02 Å compared with those associated with the $HSH\cdots SH_2$ H-bonds (refer to data supplied in the electronic supplementary information).†

The additional H_2S ligands of isomers IV and V are situated above and below the C_s symmetry tetramer core cluster. The difference in the structures is that for isomer IV the ligands are to the same side, while for isomer V they are displaced. In both isomers the top H_2S forms a H-bond to both the HF moiety and to another H_2S, while the bottom H_2S forms H-bonds to both SH^- and H_2S. For the top H_2S of isomer IV, the H-bonds to HF and H_2S are of similar strength, as the stabilisation energies are 5.9 and 4.3 kcal mol^{-1}, respectively. For the bottom H_2S however, the H-bond to the SH^- moiety is far stronger than $HSH\cdots SH_2$ bond, with the stabilisation energies being 18.1 and 1.1 kcal mol^{-1}, respectively. A similar situation is predicted from NBO calculations for isomer V.

Isomer VI is the highest energy isomer of this subset and features both ligands situated above a tetramer C_s isomer unit. The ligand to the right in Fig. 9b forms a H-bond with both the HF moiety and with the lower H_2S ligand. The stabilisation energies for these interactions are 8.5 and 4.9 kcal mol^{-1}, respectively. The ligand to the left forms H-bonds with the lower left H_2S, and also the top right H_2S with similar stabilisation energy of around 5.5 kcal mol^{-1}. Again, these interactions are shown in Fig. 9b by dashed lines.

We move now to the third subset of clusters with the $FH\cdots SH^-$–$(H_2S)_4$ form shown in Fig 9c. Isomer VII features a planar structure with only two hydrogens out of the plane. The remaining hydrogens are involved in H-bonding between the cluster constituents. The strongest intra-cluster H-bonds are for H_2S ligands to the SH^- moiety, with the strongest of these having a stabilisation energy of 31.2 kcal mol^{-1} for the H_2S ligand with the hydrogen pointing out of the plane. Not surprisingly, the predicted $S^-\cdots$HS H-bond angle is very close to linearity at 177°, leading to very good lone pair and σ* orbital overlap. For comparison, the angles of the other $S^-\cdots$HS H-bonds are less than 170°. The weakest of the H-bonds is for one of the $HF\cdots$HSH bonds, with a stabilisation energy of only 0.7 kcal mol^{-1}.

Finally, a similar situation is predicted for isomer VIII, with multiple intra-cluster H-bonds existing as shown in Fig. 9c. Again, the strongest interactions are the $HS^-\cdots$HSH hydrogen bonds with the stabilisation energies in the 12.5–23.3 kcal mol^{-1} range. The $HF\cdots$HSH hydrogen bond is predicted to be quite strong in this isomer, with a stabilisation energy of 6.8 kcal mol^{-1}. The weakest H-bonds are for the $HSH\cdots SH_2$ interactions, where in this case the stabilisation energies are 1.9 to 4.6 kcal mol^{-1}.

II. Cluster energies. As the energy separation between the lowest and highest energy isomer is only 1.9 kcal mol^{-1} at this level of theory, one cannot state definitively which isomer would be preferred. Significant error is also introduced by using zero point energies calculated from purely harmonic vibrational frequencies. From this study it appears that all of the clusters could be produced, and hence the predicted infrared spectra will become important in rationalising experimental spectra.

III. Predicted infrared spectra. The predicted vibrational frequencies for each isomer, along with associated symmetries and intensities, can be found in the electronic supplementary

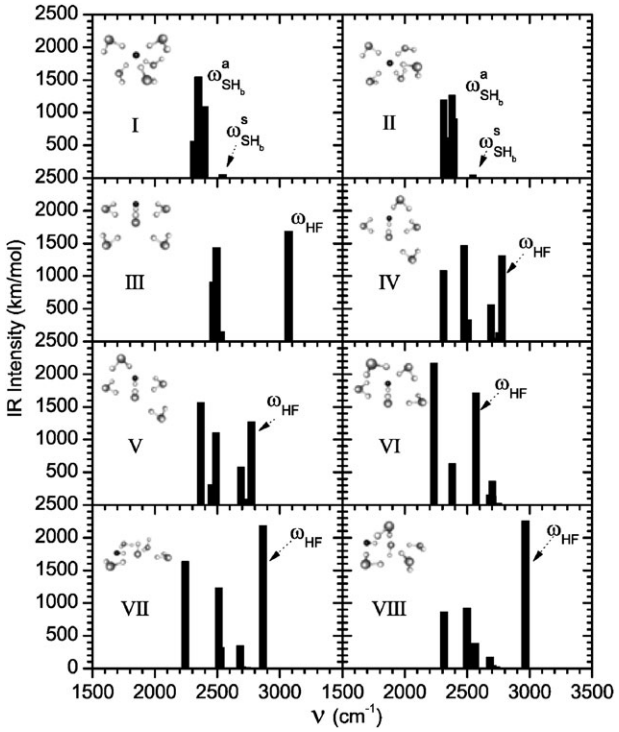

Fig. 10 Predicted infrared spectra for 1 : 5 clusters from MP2/aug-cc-pvdz calculations. The top two spectra correspond to the 'solvated F^-' type structures, while the remaining are the $FH\cdots SH^-$–$(H_2S)_4$ isomers. The full set of predicted vibrational frequencies can be found in the electronic supplementary material.†

material.† Here we concentrate on the S–H and F–H stretching regions shown as stick spectra in Fig. 10.

The most intense peaks are labelled in Fig. 10. The labels take the same format as used previously, *i.e.* $\omega_{XH}^{a/s}$ describing the mode as antisymmetric (a) or antisymmetric (s), and whether it is principally a S–H or F–H stretch. For clarity, in the predicted spectra of the $FH\cdots SH^-$–$(H_2S)_4$ type structures, only the ω_{HF} stretch has been marked. The remaining bands correspond to stretching motions of the H-bonded S–H groups.

The predicted spectra should aid in determining whether 'solvated F^-' or '$FH\cdots SH^-$' type clusters are produced experimentally, as for the former the spectra are dominated by a single broad feature composed of the various antisymmetric stretching modes of the H-bonded S–H groups. More than one intense band in the spectrum would constitute compelling evidence that the $FH\cdots SH^-$–$(H_2S)_4$ cluster form is favoured.

Finally, it is worth noting the variation in the position of common stretching vibrations between isomers, highlighting the effect of the solvent environment. For example, the position of the ω_{HF} stretching band differs significantly for the isomers containing the $FH\cdots SH^-$ core, and for isomer VI this band shifts below two of the higher wavenumber S–H stretching bands.

4. Summary

Clusters formed between a fluoride anion and several H_2S ligands have been investigated *via ab initio* calculations. We have provided structures and associated infrared spectra for clusters with up to five H_2S molecules interacting with a F^- anion. The major finding of this study is that for the smaller clusters, the dominant form is one where a proton has transferred from one of the H_2S ligands to form a $FH\cdots SH^-$ anion core. The first occurrence of a 'solvated F^-' type structure is for the $n = 3$ cluster size, however in this case the cluster form is predicted to lie some 4.6 kcal mol^{-1} above the $FH\cdots SH^-$–$(H_2S)_2$ minimum. For the F^-–$(H_2S)_4$ and F^-–$(H_2S)_5$ cluster sizes, the predicted energy separation between 'solvated F^-' and '$FH\cdots SH^-$' structures becomes much smaller.

The strength of the bonding interaction between the ligands and the ion core decreases with increased cluster size. This effect is observed in the ligand structural parameters, particularly emphasised in the shortening of the S–H bonds of the solvating H_2S ligands.

It will be interesting to see if experimental studies, particularly infrared spectroscopy, can provide support for the predicted proton transferred form of the dimer, and indeed discriminate between the two cluster types of the larger species. There are marked differences in the predicted infrared spectra which should clarify this issue.

Acknowledgements

We thank Martin Fechner (MPI) for assistance with work stations, the MPI für biophysikalische Chemie and the Alexander von Humboldt Foundation for financial support.

References

1 J. V. Coe, *Int. Rev. Phys. Chem.*, 2001, **20**, 33.
2 S. Nandi, A. Sanov, N. Delaney, J. Faeder, R. Parson and W. C. Lineberger, *J. Phys. Chem. A*, 1998, **102**, 8827.
3 M. E. Nadal, P. D. Kleiber and W. C. Lineberger, *J. Chem. Phys.*, 1996, **105**, 504.
4 C. A. Corbett, T. J. Martinez and J. M. Lisy, *J. Phys. Chem. A*, 2002, **106**, 10015.
5 M. Ichihashi, Y. Sadanaga, J. M. Lisy and T. Kondow, *Chem. Lett.*, 2000, **11**, 1240.
6 O. M. Cabarcos, C. J. Weinheimer, T. J. Martinez and J. M. Lisy, *J. Chem. Phys.*, 1999, **110**, 9516.
7 W. H. Robertson, K. Karapetian, P. Ayotte, K. D. Jordan and M. A. Johnson, *J. Chem. Phys.*, 2002, **116**, 4853.
8 W. H. Robertson, E. G. Diken, E. A. Price, J. W. Shin and M. A. Johnson, *Science*, 2003, **299**, 1367.
9 S. B. Nielsen, P. Ayotte, J. A. Kelley and M. A. Johnson, *J. Chem. Phys.*, 1999, **111**, 9593.
10 E. J. Bieske, *Chem. Soc. Rev.*, 2003, **32**, 231.
11 D. A. Wild, P. J. Milley, Z. M. Loh, P. S. Weiser and E. J. Bieske, *Chem. Phys. Lett.*, 2000, **323**, 49.
12 D. A. Wild, P. S. Weiser, E. J. Bieske and A. Zehnacker, *J. Chem. Phys.*, 2001, **115**, 824.
13 D. A. Wild, Z. M. Loh, R. L. Wilson and E. J. Bieske, *J. Chem. Phys.*, 2002, **117**, 3256.
14 S. A. Nizkorodov, O. Dopfer, T. Ruchti, M. Meuwly, J. P. Maier and E. J. Bieske, *J. Phys. Chem.*, 1995, **99**, 17118.
15 M. S. Johnson, K. T. Kuwata, C. K. Wong and M. Okumura, *Chem. Phys. Lett.*, 1996, **260**, 551.
16 J. H. Choi, K. T. Kuwata, Y. B. Cao and M. Okumura, *J. Phys. Chem. A*, 1998, **102**, 503.
17 J. H. Choi, K. T. Kuwata, B. M. Haas, Y. B. Cao, M. S. Johnson and M. Okumura, *J. Chem. Phys.*, 1994, **100**, 7153.
18 K. Seki, Y. Sumiyoshi and Y. Endo, *Chem. Phys. Lett.*, 2000, **331**, 184.
19 Y. Ohshima, Y. Sumiyoshi and Y. Endo, *J. Chem. Phys.*, 1997, **106**, 2977.
20 S. T. Arnold, J. H. Hendricks and K. H. Bowen, *J. Chem. Phys.*, 1995, **102**, 39.
21 J. H. Hendricks, H. L. de Clercq, C. B. Freidhoff, S. T. Arnold, J. G. Eaton, C. Fancher, S. A. Lyapustina, J. T. Snodgrass and K. H. Bowen, *J. Chem. Phys.*, 2002, **116**, 7926.
22 T. Lenzer, I. Yourshaw, M. R. Furlanetto, N. L. Pivonka and D. M. Neumark, *J. Chem. Phys.*, 2002, **116**, 4170.
23 T. Lenzer, I. Yourshaw, M. R. Furlanetto, N. L. Pivonka and D. M. Neumark, *J. Chem. Phys.*, 2001, **115**, 3578.
24 S. Roszak and J. Leszczynski, *J. Phys. Chem. A*, 2003, **107**, 949.
25 P. Botschwina, T. Dutoi, M. Mladenovic, R. Oswald, S. Schmatz and H. Stoll, *Faraday Discuss.*, 2001, **118**, 433.
26 A. V. Nemukhin, A. A. Granovsky and D. A. Firsov, *Mendeleev Commun.*, 1999, **6**, 215.
27 H. H. Ritze, *Chem. Phys. Lett.*, 1997, **275**, 399.
28 O. M. Cabarcos, C. J. Weinheimer, J. M. Lisy and S. S. Xantheas, *J. Chem. Phys.*, 1999, **110**, 5.
29 P. Ayotte, G. H. Weddle and M. A. Johnson, *J. Chem. Phys.*, 1999, **110**, 7129.

30 P. Ayotte, C. G. Bailey, G. H. Weddle and M. A. Johnson, *J. Phys. Chem. A*, 1998, **102**, 3067.
31 G. M. Chaban, S. S. Xantheas and R. B. Gerber, *J. Phys. Chem. A*, 2003, **107**, 4952.
32 M. Masamura, *J. Phys. Chem. A*, 2002, **106**, 8925.
33 M. Masamura, *J. Chem. Phys.*, 2003, **118**, 6336.
34 S. S. Xantheas and T. H. Dunning, Jr., *J. Phys. Chem.*, 1994, **98**, 13489.
35 S. S. Xantheas and L. X. Dang, *J. Phys. Chem.*, 1996, **100**, 3989.
36 F. N. Keutsch, J. D. Cruzan and R. J. Saykally, *Chem. Rev.*, 2003, **103**, 2533.
37 F. Huisken, M. Kaloudis and A. Kulcke, *J. Chem. Phys.*, 1996, **104**, 17.
38 W. H. Robertson and M. A. Johnson, *Annu. Rev. Phys. Chem.*, 2003, **54**, 173.
39 C. Blondel, C. Delsart and F. Goldfarb, *J. Phys. B: At. Mol. Opt. Phys.*, 2001, **34**, L281.
40 K. Rempala and K. M. Ervin, *J. Chem. Phys.*, 2000, **112**, 4579.
41 J. R. Smith, J. B. Kim and W. C. Lineberger, *Phys. Rev. A*, 1997, **55**, 2036.
42 A. J. Bell and T. G. Wright, *J. Phys. Chem. A*, 2004, **108**, 10486.
43 M. J. Travers, D. C. Cowles and G. B. Ellison, *Chem. Phys. Lett.*, 1989, **164**, 449.
44 D. A. Wild and T. Lenzer, *Phys. Chem. Chem. Phys.*, 2004, **6**, 5122.
45 R. Ayala, J. M. Martinez, R. R. Pappalardo and E. S. Marcos, *J. Chem. Phys.*, 2003, **119**, 9538.
46 S. S. Xantheas, *J. Phys. Chem.*, 1996, **100**, 9703.
47 P. Weis, P. R. Kemper, M. T. Bowers and S. S. Xantheas, *J. Am. Chem. Soc.*, 1999, **121**, 3531.
48 R. A. Kendall, T. H. Dunning and R. J. Harrison, *J. Chem. Phys.*, 1992, **96**, 6796.
49 D. E. Woon and T. H. Dunning, *J. Chem. Phys.*, 1993, **98**, 1358.
50 T. H. Dunning, *J. Chem. Phys.*, 1989, **90**, 1007.
51 S. F. Boys and F. Bernardi, *Mol. Phys.*, 1970, **19**, 553.
52 A. E. Reed, L. A. Curtiss and F. Weinhold, *Chem. Rev.*, 1988, **88**, 899.
53 J. E. Del Bene, H. D. Mettee, M. J. Frisch, B. T. Luke and J. A. Pople, *J. Phys. Chem.*, 1983, **87**, 3279.
54 M. J. Frisch, G. W. Trucks, H.B. Schlegel, G. E. Scuseria, M. A. Robb, J. R. Cheeseman, J. A. Montgomery, Jr., T. Vreven, K. N. Kudin, J. C. Burant, J. M. Millam, S. S. Iyengar, J. Tomasi, V. Barone, B. Mennucci, M. Cossi, G. Scalmani, N. Rega, G. A. Petersson, H. Nakatsuji, M. Hada, M. Ehara, K. Toyota, R. Fukuda, J. Hasegawa, M. Ishida, T. Nakajima, Y. Honda, O. Kitao, H. Nakai, M. Klene, X. Li, J. E. Knox, H. P. Hratchian, J. B. Cross, V. Bakken, C. Adamo, J. Jaramillo, R. Gomperts, R. E. Stratmann, O. Yazyev, A. J. Austin, R. Cammi, C. Pomelli, J. Ochterski, P. Y. Ayala, K. Morokuma, G. A. Voth, P. Salvador, J. J. Dannenberg, V. G. Zakrzewski, S. Dapprich, A. D. Daniels, M. C. Strain, O. Farkas, D. K. Malick, A. D. Rabuck, K. Raghavachari, J. B. Foresman, J. V. Ortiz, Q. Cui, A. G. Baboul, S. Clifford, J. Cioslowski, B. B. Stefanov, G. Liu, A. Liashenko, P. Piskorz, I. Komaromi, R. L. Martin, D. J. Fox, T. Keith, M. A. Al-Laham, C. Y. Peng, A. Nanayakkara, M. Challacombe, P. M. W. Gill, B. G. Johnson, W. Chen, M. W. Wong, C. Gonzalez and J. A. Pople, *GAUSSIAN 03 (Revision B.04)*, Gaussian, Inc., Wallingford, CT, 2003.
55 L. Laaksonen, *J. Mol. Graphics*, 1992, **10**, 33.
56 D. L. Bergman and L. Laaksonen, *J. Mol. Graphics Modell.*, 1997, **15**, 301.
57 D. A. Wild and T. Lenzer, in preparation.
58 J.-O. Jung and R. B. Gerber, *J. Chem. Phys.*, 1996, **105**, 10332.
59 M. W. Schmidt, K. K. Baldridge, J. A. Boatz, S. T. Elbert, M. S. Gordan, J. H. Jensen, S. Koseki, N. Matsunaga, K. A. Nguyen, S. J. Su, T. L. Windus, M. Dupuis and J. A. Montgomery, *J. Comput. Chem.*, 1993, **14**, 1347.
60 P. Ayotte, S. B. Nielsen, G. H. Weddle, M. A. Johnson and S. S. Xantheas, *J. Phys. Chem. A*, 1999, **103**, 10665.
61 H. E. Dorsett, R. O. Watts and S. S. Xantheas, *J. Phys. Chem. A*, 1999, **103**, 3351.
62 T. H. Edwards, N. K. Moncur and L. E. Snyder, *J. Chem. Phys.*, 1967, **46**, 2139.
63 G. di Londardo and A. E. Douglas, *Can. J. Phys.*, 1973, **51**, 434.
64 M. Gruebele, M. Polak and R. J. Saykally, *J. Chem. Phys.*, 1987, **86**, 1698.
65 G. C. Pimentel and A. L. McClellan, *The Hydrogen Bond*, ed. W. H. Freeman, New York, 1960.
66 D. A. Wild, Z. M. Loh, R. L. Wilson and E. J. Bieske, *Chem. Phys. Lett.*, 2003, **369**, 684.

